COMPRESSION AND BENDING BEHAVIOR OF STEEL FIBER REINFORCED SELF-COMPACTING CONCRETE

E.B. Pereira[1], J.A.O. Barros [1], V.M.C.F. Cunha [1] and S.P.F. Santos [2]

[1]University of Minho, Portugal
[2]Civitest Company, Portugal

Abstract
A method to design cost competitive steel fiber reinforced self-compacting concrete (SFRSCC) for precasting industrial applications is described in this paper. Since demolding the elements as soon as possible is an important requirement in this industry, the influence of the age on the resistance and toughness of the designed SFRSCC was assessed carrying out an experimental program. Based on the force-deflection relationship obtained in the three point bending notched beam tests performed according to the RILEM TC 162-TDF recommendations, the stress-crack opening relationship of the SFRSCC was determined. The influence of the SFRSCC age on the fracture parameters of this material was analyzed.

Keywords: *Self-compacting concrete, steel fibers, post-cracking behavior.*

Eduardo Borges Pereira
Assistant
University of Minho
Department of Civil Engineering
School of Engineering
4800-058 Guimarães
Portugal

Email: epereira@civil.uminho.pt
Tel.: (+351) 253 510 248

1 Introduction

The concrete precasting industry is frequently confronted with the production of structural reinforced concrete elements of some geometric complexity. These geometric conditions introduce difficulties on the placement of the reinforcement, resulting in a large consuming time phase of the industrial process. Moreover, when high percentage of reinforcement is used, there are difficulties on assuring the desired concrete pouring quality, resulting in deficiencies that can compromise the mechanical behavior and the visual appearance of the final structure.

Self-compacting concrete (SCC) can be defined as concrete that is able to flow in the interior of the formwork, passing through the reinforcement and filling it in a natural manner, being consolidated under the action of its own weight. Adding the benefits of SCC to those resulting from the addition of discrete fibers to cement based materials, a high performance material, designated by steel fiber reinforced self-compacting concrete (SFRSCC), is obtained.

The present work is part of a research program for the development of lightweight sandwich SFRSCC panels for precasting industry. The requirements established for this SFRSCC were the following: average compression strength at 24 hours greater than 20 MPa; equivalent flexural tensile strength [1] greater than 2 MPa at this age; content of cement not exceeding 400 Kg/m^3; the cement should be the most expensive component of the binder paste. The strategy followed to design this SFRSCC is briefly described in the present paper.

In the precasting industry, the ability to demold the elements as soon as possible is an important requirement. To assure safe demolding process, the influence of the concrete age on the flexural and compression behavior of the SFRSCC should be known. For this purpose, an experimental program was carried out with specimens of 12 hours, 24 hours, 3, 7 and 28 days. Special care was taken to evaluate the post-cracking behavior of the SFRSCC [2], since the fracture mode I crack constitutive law was derived from the results obtained in these flexural tests, and used in a discrete crack model implemented into a computational code based on the finite element method (FEM) that is able to simulate the nonlinear behavior of concrete structures [3]. The experimental program is described and the results are presented and analyzed.

2 Method for Preparing SFRSCC

The materials used were cement (C) CEM I 42.5R (rapid hardening and high strength cement, according to European Norm EN197-1:1998), limestone filler (LF), superplasticizer (SP) of third generation based on polycarboxilates (Glenium® 77SCC), water (W), three types of aggregates (fine river sand, coarse river sand and crushed granite 5-12 mm) and DRAMIX® RC-80/60-BN hooked end steel fibers. This fiber has a length (l_f) of 60 mm, a diameter (d_f) of 0.75 mm, an aspect ratio (l_f/d_f) of 80 and a yield stress of 1100 MPa. The method developed in the present work is based on the three following steps: i) the proportions of the constituent materials of the binder paste are defined; ii) the proportions of each aggregate on the final solid skeleton are determined; iii) binder paste and solid skeleton are mixed in different proportions until self-compacting requirements in terms of spread ability, correct flow velocity, filling ability, blockage and segregation resistance are assured.

In the first step, a series of tests were performed to achieve the optimum composition of the binder paste. To define the optimum percentage of LF addition in the final composition, several mixes of LF, cement and water were prepared. The proportions of each component were defined in terms of volume, the water content was 66% of cement volume, and the percentage of LF has varied between 0% and 125% of the cement volume. To promote the

dispersion and deflocculation of the fine particles in suspension [2], a small constant quantity of superplasticizer was also added to each mix. The relative spread in the "Flow table" and the “Marsh cone” flow time of each mix were measured. Concluding the paste phase design, the compression strength of each mix was also evaluated on 5 cm edge cubic specimens at an age of 7 days. A percentage of 100% of LF relative to the cement volume has resulted in a good compromise between strength and flowability requirements, and has also allowed maintaining the amount of cement on the final concrete mix only slightly above 350 kg/m^3.

In the second step, the most appropriate proportions of the three types of aggregates were obtained preparing mixes of distinct quantities of each type of aggregate, and weighting 5 dm^3 volume for each mix. The optimum aggregate mix was assumed to be the heaviest one, since it should correspond to the most compact. An estimated portion of fibers equivalent to 30 Kg of fibers per m^3 of concrete was included in every mixture. Initially, only two of the three types of aggregates were mixed. After finding the optimum relation between these two, the third aggregate was added in distinct volumetric percentages, keeping constant the relation between the two first aggregates. These results indicated that the optimum solid skeleton was composed, in volume, by 49.5% of coarse sand, 40.5% of crushed stone and 10% of fine sand.

The third phase is dedicated to the evaluation of the paste content in the concrete volume. The optimum composition should accomplish an upper limit of around 350 kg of cement per m^3 of concrete. To achieve the optimum paste content, some mixes of concrete were prepared, varying the paste percentage. For each mix, the added water was evaluated taking into account the aggregate’s saturation degree. The mix process was always the same, and for each mix the slump flow test was performed. Total spread, s, and time to reach a spread diameter of 500 mm, T_{50}, were measured. Table 1 includes the composition that has best fitted self-compacting requirements (the amount of water referred includes the aggregate’s saturation water). No sign of segregation was detected, a total spread of 725 mm was measured and the mixture showed good homogeneity and cohesion, even when flowing trough the small orifice of the Abrams cone (when testing, Abrams cone was always used in the inverted position). A T_{50} of 4.6 seconds was measured.

Table 1: Final composition for 1 m^3 of SFRSCC made with 30 kg/m^3 of fibers

Paste/Total volume (%)	Cement (kg)	LF (kg)	Water (dm^3)	SP (dm^3)	Fine sand (kg)	Coarse sand (kg)	Crushed aggregates (kg)
0.34	364.28	312.24	139.12	6.94	108.59	723.96	669.28

3 SFRSCC Mechanical Properties

The experimental program was composed of uniaxial compression tests with cylinders of 150 mm diameter and 300 mm height, and flexural tests with prismatic 600×150×150 mm^3 specimens. Both types of specimens were molded without any external compaction energy. To assess the influence of the age of the SFRSCC on the compression and on the flexural behavior, series of tests with specimens of 12 and 24 hours, and 3, 7 and 28 days were carried out.

3.1 Compression

The compression tests were carried out in a servo-controlled equipment of 3000 kN maximum load carrying capacity. Each test was controlled by the internal displacement transducer of this equipment, at a displacement rate of 5 μm/s. Three displacement transducers were positioned at 120 degrees around the specimen and registered the displacements between the load steel platens of the equipment (see Figure 1). This test setup avoids that the deformation of the test equipment is added to the values read by the LVDTs.

Taking the values recorded in these transducers, the displacement at the specimen axis was determined for each scan reading [4], and the corresponding strain was obtained dividing this displacement by the measured specimen's height. The compression stress-strain relationship, $\sigma_c - \varepsilon_c$, for each testing age of the SFRSCC is represented in Figure 2. Each curve is the average of three specimens. As it was expected, the decay of the post-peak residual compression strength has increased with the SFRSCC age, since the material becomes more brittle with the increase of the compression strength. However, this decay is not as pronounced as it will be expected for plain concrete.

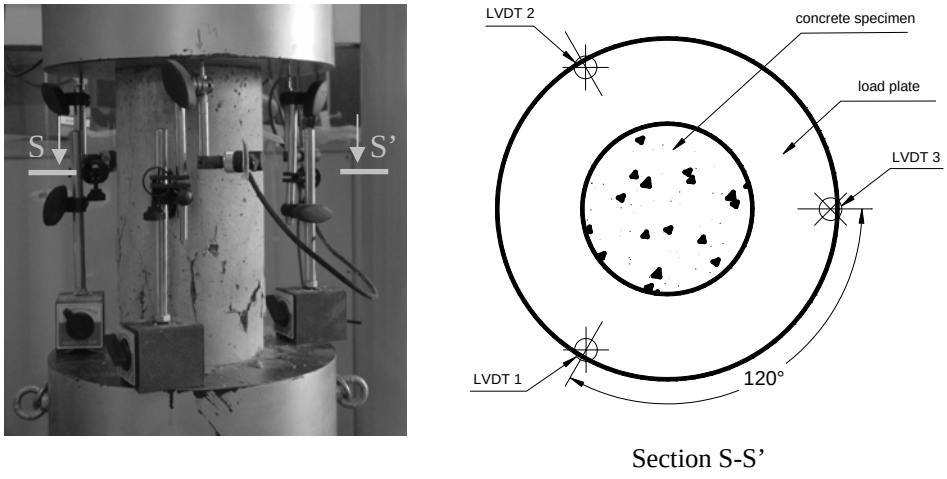

Figure 1 – Setup of the direct compression test.

Figure 3 checks if the $\sigma_c - \varepsilon_c$ expressions proposed by CEB-FIP 1993 [5] to simulate the uniaxial compression behavior of plain concrete can be applicable to the designed SFRSCC. This figure shows that those expressions simulate with high accuracy the uniaxial compression behavior of the conceived SFRSCC up to its peak stress, but in the softening phase (post-peak) they predict a stress decay higher than the one observed experimentally.

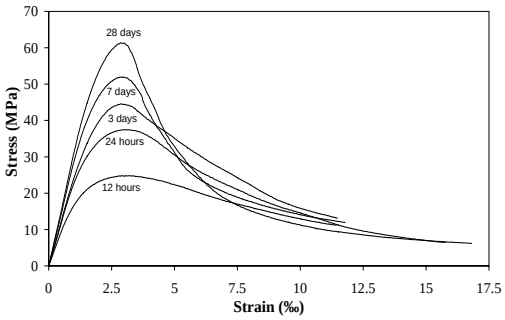

Figure 2. Stress-strain curves for SFRSCC cylinder specimens of distinct age at testing.

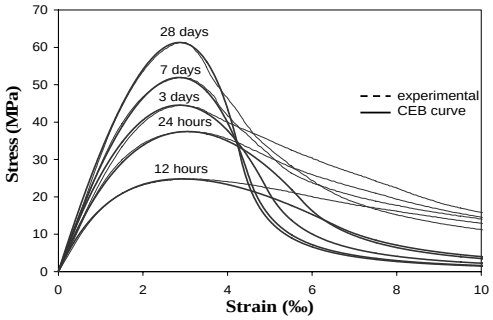

Figure 3. Assessing the ability of the CEB-FIP 1993 expressions to simulate the SFRSCC uniaxial compression behavior.

Figure 4 and Figure 5 show the influence of the age on the average compressive strength, f_{cm}, and on the average initial Young's Modulus, E_{cm}. From the analysis of these figures, the following observations can be pointed out: at 12 hours the pre-established minimum limit of 20 MPa for the compressive strength at 24 hours has already been exceeded. At this age the f_{cm} was about 25 MPa while the E_{cm} was around 24 GPa. These properties increased with the SFRSCC age, reaching f_{cm} = 62 MPa and E_{cm} = 36 GPa at 28 days. The evolution of the

compression strength with time indicates that above 28 days the increase of the f_{cm} is marginal. This can be justified by the use of relatively high percentage of a material (limestone filler) without pozolanic activity in the binder paste composition. The evolution of the Young's Modulus with the age indicates that above 28 days the increase of the E_{cm} is marginal. This can be justified by the low value of the water/cement ratio (approximately 0.28 in weight), since a high compact matrix has resulted. At 24 hours the f_{cm} and the E_{cm} were about 61% and 79% of the corresponding values at 28 days. In the first hours, there was a more pronounced increase in E_{cm} than in f_{cm}.

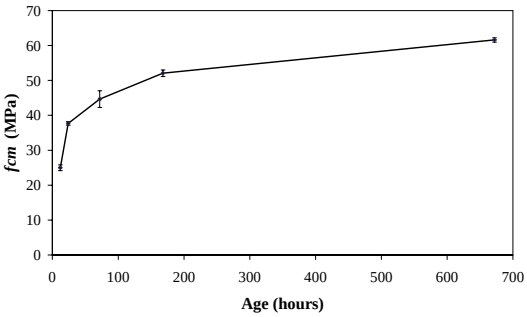

Figure 4. Influence of the SFRSCC age on its average compressive strength.

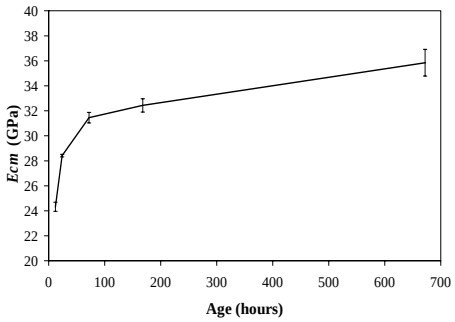

Figure 5. Influence of the SFRSCC age on its initial Young's modulus.

3.2 Bending

In the bending tests, the curing procedures, the position and dimensions of the notch sawn into the specimen, the load and specimen support conditions, the characteristics for both the equipment and measuring devices, and the test procedures recommended by RILEM TC 162-TDF [1] were adopted. The method for casting the beam specimens proposed by RILEM TC 162-TDF was adapted for SFRSCC since they were cast without any external compaction energy.

In order to evaluate the flexural performance of the testing specimens in distinct limit states, according to RILEM TC 162-TDF [1] two types of variables are determined. The first type is more related to the shape of the load-deflection curve, and includes the F_L, $F_{R,1}$, F_2, F_3 and $F_{R,4}$, and the second type is associated with the energy dissipated during fracture process, and includes mainly the $f_{eq,2}$ and $f_{eq,3}$ values. F_L value corresponds to the highest value of the load recorded up to a deflection at midspan of the test beam of 0.05 mm, and its determination is performed numerically, being δ_L the deflection at midspan when F_L value is reached. $F_{R,1}$, F_2, F_3 and $F_{R,4}$ correspond respectively to the load value registered to a deflection at midspan of 0.46 mm ($\delta_{R,1}$), 0.7 mm (δ_2), 2.7 mm (δ_3) and 3 mm ($\delta_{R,4}$). $f_{eq,i}$ values correspond to the maximum stress values reached at midspan section, considering a linear elastic diagram of stress distribution (triangular diagram), and relating the moment at midspan with the area of the load-deflection diagram, up to a deflection level of δ_L +0.65mm in the case of $f_{eq,2}$, and up to a deflection level of δ_L +2.65mm in the case of $f_{eq,3}$.

The force-deflection curves, F-δ, obtained in the tested series are depicted in Figure 6. Each curve is the average of the F-δ relationship recorded in three specimens. The influence of the SFRSCC age in the force corresponding to the limit of proportionality, F_L, is graphically represented in Figure 7. As shown in figure 7, F_L increased with the SFRSCC age, but this increase became marginal after 7 days.

Just after deflection at midspan value reached δ_L a load decay occurred with an amplitude that increased with the SFRSCC age (see Figure 6), since a higher load should be sustained by the fibers bridging mechanism at the specimen's fracture surface. This load decay was followed by a hardening phase up to a deflection level that has decreased with the SFRSCC age. Except for specimens of 28 days, in the remaining the maximum load was larger than F_L. Apart series of 12 hours, in the remaining series the hardening phase was followed by a softening branch. The decrease of residual strength in the softening branch was much more significant in series

of specimens of 28 days. The larger amplitude of load decay just after reaching δ_L in this series would have adversely affected the fiber-concrete bond properties and the fiber anchorage efficacy, leading to a decrease in the force necessary to pullout the fibers crossing the specimen fracture surface. As a result, the equivalent (f_{eq}) and the residual (f_R) flexural tensile strength parameters [1] have only decreased between 7 and 28 days, as seen in Figure 8. This decrease was more pronounced in the $f_{R,4}$ since this parameter is directly dependent on the shape of the force-deflection curve, and is evaluated for a deflection of 3.0 mm. As $f_{eq,2}$ and $f_{R,1}$ had similar variation with the age, this means that, for low values of deflection (δ_2 and $\delta_{R,1}$), the energy and the force based concepts provide identical results.

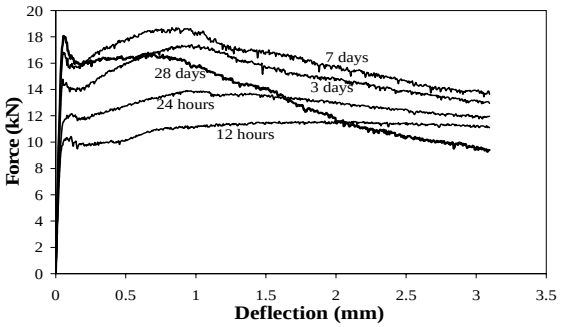

Figure 6. Force-deflection curves for SFRSCC notched beam specimens of distinct age at testing.

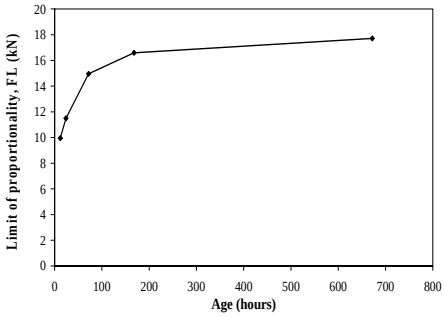

Figure 7. Influence of the SFRSCC age on the F_L.

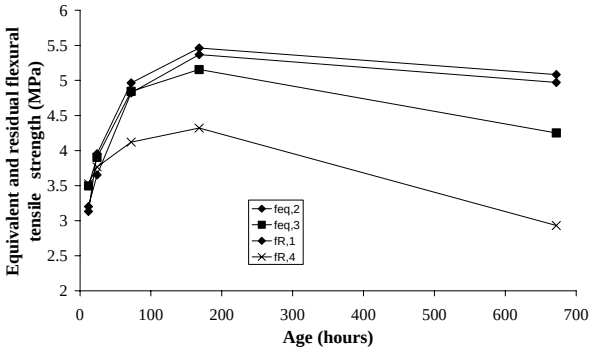

Figure 8. Influence of the SFRSCC age on the equivalent and residual tensile strength parameters.

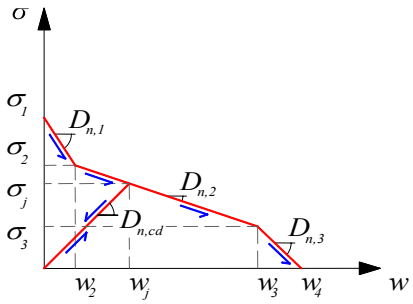

Figure 9. Adopted stress-crack opening diagram.

4 Fracture Parameters of the SFRSCC

Previous research has shown that the post-cracking behavior of SFRC materials can be simulated by the trilinear stress-crack opening diagram, σ-*w*, represented in Figure 9 [2, 3]. To evaluate the influence of the SFRSCC age on the values of the fracture parameters of this material, an inverse analysis was carried out in order to obtain the dependence of the σ_i and w_i, that define the σ-*w* diagram, on the age of the SFRSCC. Knowing these dependencies, the influence of the SFRSCC age on its fracture energy [6] can be directly derived.

The inverse analysis was performed evaluating the values of the σ_i and w_i that best fit the experimental F-δ curves with the minimum error of the parameter,

$$err = \left| A_{F-\delta}^{\exp} - A_{F-\delta}^{num} \right| \Big/ A_{F-\delta}^{\exp} \qquad (1)$$

where $A_{F-\delta}^{\exp}$ and $A_{F-\delta}^{num}$ are the areas below the experimental and the numerical F-δ curves, respectively. For this purpose, a computational code named FEMIX was used, that has discrete and smeared crack models to simulate the crack initiation and crack propagation in cement based materials [7]. Since the RILEM TC 162-TDF flexural test brings up a localized fracture problem, a discrete crack model, described in detail elsewhere [3], was used. Six-node 2D line interface finite elements were located in the specimen's symmetry axis to model the fracturing process, see Figure 10. In the remaining parts of the specimen, eight-node Serendipity linear-elastic plane-stress elements were used. Gauss-Lobatto integration scheme 3 with three integration points (IP) was used for the 2D line interface finite elements, while Gauss-Legendre integration scheme with 2×2 IP was used for the eight-node elements. To avoid undesired spurious oscillations of the stress field, a value of 1.0×10^4 N/mm^3 was assigned to the initial mode I stiffness for the interface element 3. Since sliding between the fracture surfaces does not occur in this type of problem, the analysis is independent of the values assigned to the mode II stiffness of the interface element.

The adequacy of the numerical strategy adopted is shown in Figure 11, revealing that the proposed trilinear σ-w diagram is capable of predicting, with enough accuracy, the post-cracking behavior of the tested specimens. The values for σ_i and w_i are included in Table 2 and correspond to the simulation of the average F-δ experimental curves.

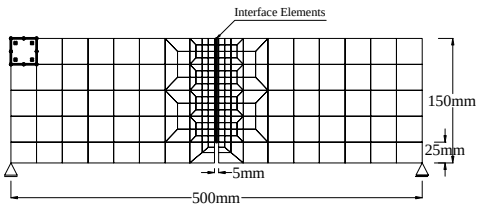

Figure 10. Finite element mesh.

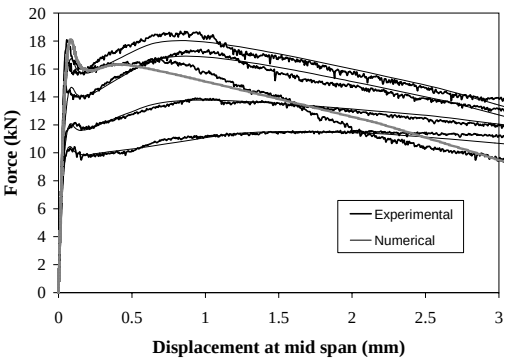

Figure 11. Experimental vs. numerical F-δ curves.

Table 2. Fracture parameters for SFRSCC of distinct ages

Age (days)	σ_1 (MPa)	w_2 (mm)	σ_2/σ_1	w_3 (mm)	σ_3/σ_1	w_4 (mm)	G_f (N/mm)
0.5	1.52	0.06	0.7	1	0.85	9	6.37
1	1.80	0.06	0.7	0.5	0.88	8	6.62
3	2.25	0.06	0.68	0.5	0.88	5	5.31
7	2.60	0.06	0.65	0.5	0.80	5	5.64
28	2.92	0.06	0.58	0.25	0.62	4	3.90

As Figure 12 shows, σ_i increase up to 7 days. After this age, σ_1 continues to increase, σ_2 maintains practically constant, and σ_3 decreases. From Figures 13 and 14 it seems that the age has a tendency to reduce the values of the w_3 and w_4, while w_2 is not affected by the age of the specimen. This means that the slope of the first softening branch of the σ-w diagram, $D_{n,1}$, increases with the ages, see Figures 9 and 15. Similar tendency was observed in the $D_{n,3}$, see Figures 9 and 17, but the increase after 3 days was not so pronounced. The variation of the $D_{n,2}$ with the age is represented in Figure 16, reflecting a hardening effect of increasing value up to 3 days, followed by a reduced decrement after this age (see also Figure 6).

The higher inclination of the softening branches and the smaller amplitude of the "hardening" branch of the σ-*w* diagram of the specimens of 28 days reflect the more brittle character of the *F*-δ response registered in these specimens.

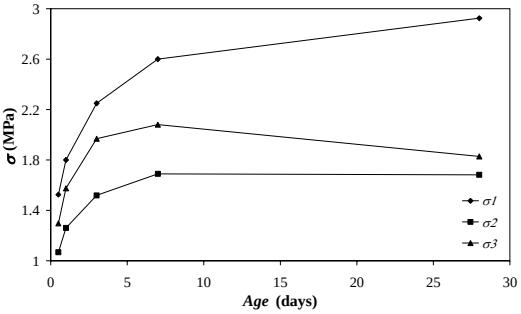

Figure 12. Influence of the SFRSCC age on the parameter σ_i

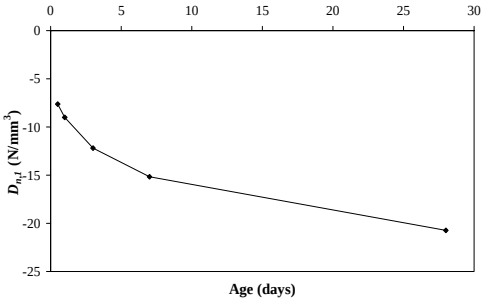

Figure 15. Influence of the age on the parameter $D_{n,1}$

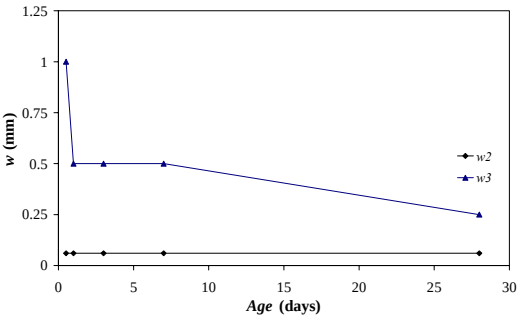

Figure 13. Influence of the SFRSCC age on the parameters w_2 and w_3.

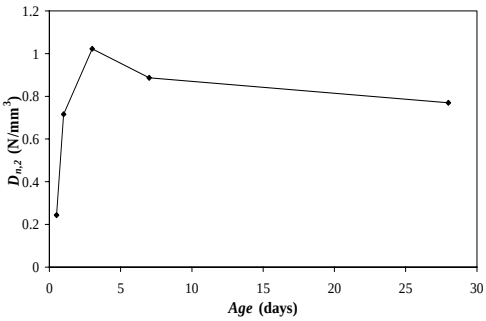

Figure 16. Influence of the age on the parameter $D_{n,2}$

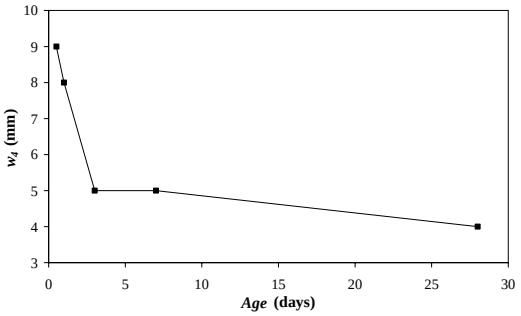

Figure 14. Influence of the SFRSCC age on the parameter w_i.

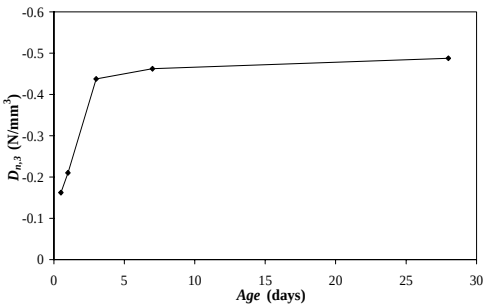

Figure 17. Influence of the age on the parameter $D_{n,3}$.

For modeling the contribution of the fiber reinforcement, the TC 162-TDF recommended the use of $f_{R,4}$ for the ultimate limit state analysis. The $f_{R,4}$ is the stress for a deflection of 3.0 mm. Therefore, only the fracture energy dissipated up to this deflection, $G_{f,3mm}$, has interest from the design point of view. The influence of the SFRSCC age on the evolution of the $G_{f,3mm}$ is represented in Figure 18, from which it can be concluded that $G_{f,3mm}$ increases up to 7 days, followed by a significant decrease after this age. This means that the fiber reinforcing mechanisms were not sufficiently benefited by the increase of the matrix strength with the age in order to assure the tendency observed in the specimens tested up to 7 days. To avoid the decrease of the $G_{f,3mm}$ after 7 days, a higher content of fibers should be applied.

Figure 19 shows that an high correlation exists between σ_1 and $f_{ctk,min}$, having $f_{ctk,min}$ been evaluated according to the CEB-FIP recommendations (1993).

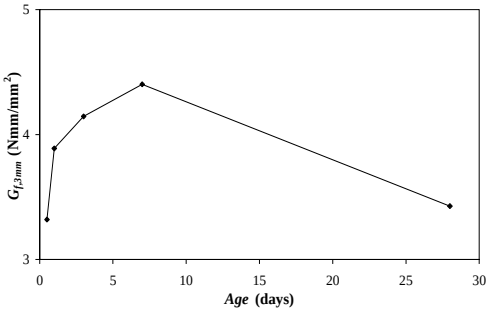

Figure 18. Influence of the SFRSCC age on the $G_{f,3mm}$

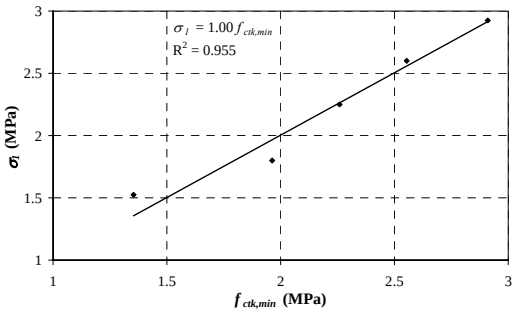

Figure19. Relationship between σ_1 and $f_{ctk,min}$.

According to TC 162-TDF, σ_2 is linearly dependent of the $f_{eq,2}$ or $f_{R,1}$, while σ_3 is linearly dependent of the $f_{eq,3}$ or $f_{R,4}$. The σ_2 -$f_{eq,2}$, σ_2 - $f_{R,1}$ and σ_3 -$f_{eq,3}$ dependencies are confirmed in figures 20 to 22, but Figure 23 indicates that a σ_3 - $f_{R,4}$ dependence was not assured. The scalar values of the σ_2 - $f_{eq,2}$ and σ_3 - $f_{eq,3}$ dependencies are, however, distinct to those proposed by TC 162-TDF for the SFRC (0.45 and 0.37, respectively, while 0.32 and 0.40 were obtained for the SFRSCC).

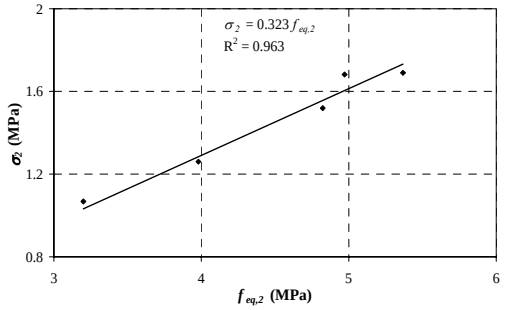

Figure 20. Relationship between σ_2 and $f_{eq,2}$.

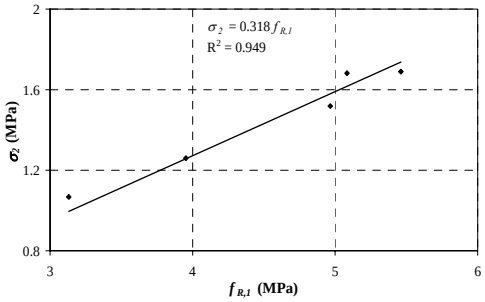

Figure 21 Relationship between σ_2 and $f_{R,1}$.

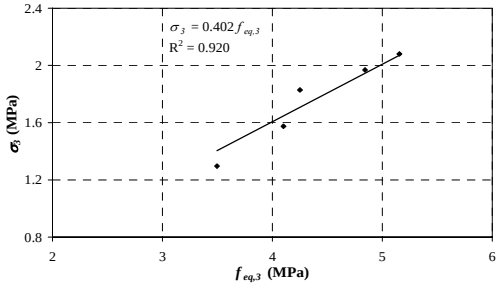

Figure 22. Relationship between σ_3 and $f_{eq,3}$.

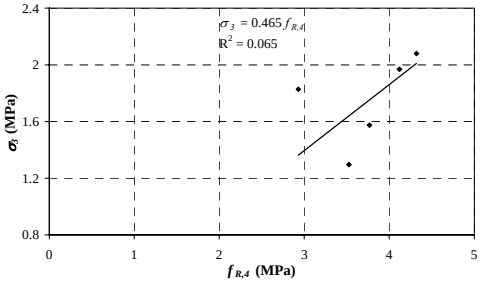

Figure 23. Relationship between σ_3 and $f_{R,4}$.

5 Conclusions

In the present work a method for cost competitive steel fiber reinforced self-compacting concrete (SFRSCC) was described. The conceived SFRSCC has attained all the requirements of self-compatibility, and compression strength of 25 MPa at 12 hours and 62 MPa at 28 days, with a content of cement of about 360 kg/m^3.

To assess the influence of the age on the compression and bending behavior of the conceived SFRSCC, an experimental program was carried out, testing specimens at 1/2, 1, 3, 7 and 28 days. The strength and ductility levels required by precasting industry for the application in which the designed SFRSCC will be used, were exceeded. Special research effort was done to assess the influence of the SFRSCC age on the mode I fracture parameters of this material. Taking the force-deflection relationships ($F-\delta$) obtained in the three point bending tests with SFRSCC notched beams and performing an inverse analysis with a discrete crack model, a trilinear stress-crack opening diagram ($\sigma-w$) was obtained for the distinct ages considered. The obtained $F-\delta$ relationships show that, to maintain the post-cracking residual force up to a deflection of 3 mm, a higher content of fibers should be used (45 kg/m^3 seems to be an adequate fiber content for this purpose). The influence of the SFRSCC age on the σ_i, w_i values defining the $\sigma-w$ diagram was analyzed, as well as, on the corresponding fracture energy. A correspondence between the σ_i values of the $\sigma-w$ diagram and the equivalent and residual flexural tensile strength parameters (f_{eq} and f_R, respectively) proposed by RILEM TC 162-TDF was obtained in order to check the applicability of the post-cracking diagram proposed by this committee for the design of SFRC. A good correlation was obtained between the σ_i and f_{eq} but the constants of this correlation were not equal to those recommended by RILEM TC 162-TDF for the current SFRC. New values were proposed for the SFRSCC mixes designed here.

6 Acknowledgments

The study reported in this paper forms a part of the research program “Prefabricated sandwich steel fiber reinforced panels” supported by FEDER and MCT, and promoted by ADI (the funds was 45% of the applied amount). This project involves the Companies PREGAIA and CIVITEST and the University of Minho. The authors wish to acknowledge the materials generously supplied by MBT (superplasticizer), SECIL (cement), Bekaert (fibers) and Comital (limestone filler).

7 References

1. Vandewalle, L. et al. 2002. Test and design methods for steel fibre reinforced concrete - Final Recommendation. Materials and Structures 35(253): 579-582.

2. Pereira, E.B.; Barros, J.A.O.; Ribeiro, A.F.; Camões, A.F.F.L., "Post-cracking behaviour of selfcompacting steel fibre reinforced concrete", 6th International RILEM Symposium on fibre reinforced concrete - BEFIB 2004, Vol. 2, pp. 1371-1380, Edts. M. di Prisco, R. Felicetti, G.A. Plizarri, 20-22 de Setembro, 2004.

3. Sena-Cruz, J.M., Barros, J.A.O., Fernandes, A., Azevedo, A.F.M. & Camões, A.F.F.L., “Stress-crack opening relationship of enhanced performance concrete”, 9th Portuguese Conference on Fracture, Setúbal, Portugal, 18-20 February 2004.

4. Untiveros, C. M. A. 2002. Estudio experimental del comportamiento del hormigón confinado sometido a compresión, PhD Thesis, UPC, Barcelona.

5. CEB-FIP Model Code 1993. Comite Euro-International du Beton, Bulletin d’Information nº 213/214.

6. RILEM Draft Recommendation, 50-FMC Committee Fracture Mechanics of Concrete 1985. Determination of the fracture energy of mortar and concrete by means of three-point bending tests on notched beams. Materials and Structures 85(85), 285-290.

7. Sena-Cruz, J.M.; Barros, J.A.O., Azevedo, A.F.M., "Elasto-plastic multi-fixed smeared crack model for concrete", Technical report 04-DEC/E-05, Dep. Civil Eng., University of Minho, 70 pp, June 2004.